Vibrational dynamics and boson peak in a supercooled polydisperse liquid

Sneha Elizabeth Abraham* and Biman Bagchi†
Solid State and Structural Chemistry Unit, Indian Institute of Science, Bangalore 560 012, India
(Received 15 June 2009; revised manuscript received 21 January 2010; published 26 March 2010)

Vibrational density of states (VDOS) in a supercooled polydisperse liquid is computed by diagonalizing the Hessian matrix evaluated at the potential energy minima for systems with different values of polydispersity. An increase in polydispersity leads to an increase in the relative population of localized high-frequency modes. At low frequencies, the density of states shows an excess compared to the Debye squared-frequency law, which has been identified with the boson peak. The height of the boson peak increases with polydispersity and shows a rather narrow sensitivity to changes in temperature. While the modes comprising the boson peak appear to be largely delocalized, there is a sharp drop in the participation ratio of the modes that exist just below the boson peak indicative of the quasilocalized nature of the low-frequency vibrations. Study of the difference spectrum at two different polydispersity reveals that the increase in the height of boson peak is due to a population shift from modes with frequencies above the maximum in the VDOS to that below the maximum, indicating an increase in the fraction of the unstable modes in the system. The latter is further supported by the facilitation of the observed dynamics by polydispersity. Since the strength of the liquid increases with polydispersity, the present result provides an evidence that the intensity of boson peak correlates positively with the strength of the liquid, as observed earlier in many experimental systems.

DOI: 10.1103/PhysRevE.81.031506 PACS number(s): 63.50.Lm, 64.70.pm

I. INTRODUCTION

A glass behaves mechanically like a solid but structurally like a liquid with relaxation times varying from a few minutes to several centuries. The elasticity of a solid is described in terms of phonons, which are quantized vibrational excitations. Propagating acoustic phononlike excitations have been observed in glasses and glass-forming liquids [1]. However, their description is rendered difficult since glasses lack the translational invariance of crystalline solids. A ubiquitous feature in the physics of glasses is the anomalous behavior of the low-frequency part of the vibration spectrum and the corresponding thermal properties [2]. While the origin of the linear low-temperature specific heat is commonly attributed to the existence of double-well potentials or two-level systems, there is a considerable debate about the so-called *boson peak* [3,4]. This peak shows up in the vibrational density of states (VDOS), $g(\nu)$ as an excess contribution, compared to the usual Debye behavior [$g(\nu) \propto \nu^2$]. It is called boson peak because the temperature-dependence of its intensity scales roughly with the Bose-Einstein distribution. In addition to the presence of boson peak (BP) (or excess density of states) at low frequencies, one also observes a high-frequency exponential tail [5] in the reduced density of states spectrum.

The interpretation of the boson peak has been a challenge to experimentalists and theoreticians and is a subject of controversial discussions. While some authors attribute it to local/quasilocal vibrations [3,6–8], some others attribute it to collective motions [5,9]. Optical heterodyne-detected optical Kerr effect data on supercooled acetylsalicylic acid and dibutylpthalate display highly damped oscillations with a period of a few picoseconds as the temperature is reduced to and below the mode coupling theory temperature, T_{MCT} [10]. The authors interpret this as the time domain signature of the boson peak and explain that the increased translational-rotational coupling is responsible for the boson peak as $T < T_{\mathrm{MCT}}$. A universal mechanism of the BP formation in glasses has been proposed based on the concept of interacting quasilocal oscillators [8]. Boson peak has also been explained in terms of the affine-nonaffine crossover at a certain mesoscopic length scale [11]. It has also been interpreted as the signature of a phase transition in the space of the stationary points of the energy, from a minima-dominated phase (with phonons) at low energy to a saddle dominated phase (without phonons) [12]. The boson peak has also been linked to those motions giving rise to the two-level-like excitations seen at still lower temperatures [13]. A recent numerical study [14] has shown that the frequency of boson peak is equal to the Ioffe-Regel limit for transverse phonons above which transverse phonons do not propagate, and the boson peak is attributed to transverse vibrational modes associated with defective soft structures in the disordered state.

Various groups have studied the vibrational dynamics of supercooled liquids [15–18] via computer simulations, where the focus has been on the characteristics of the high-frequency or low-frequency vibrational modes. The main emphasis of these studies have been on the collective/local nature of the vibrational modes. In this study, we investigate the vibrational dynamics and boson peak in a polydisperse Lennard-Jones (LJ) liquid which is one of the simplest model systems that exhibit glass transition and can be conveniently studied via both experiments [19,20] and computer simulations as the size distribution of particles prevents crystallization [21–23]. The rest of the paper is organized as follows. In Sec. II, we describe the model and computational details. In Sec. III, we present our results and give detailed discussions on the same. We give our concluding remarks in Sec. IV.

*Present address: Department of Chemistry, University of Cambridge, CB2 1EW.
†bbagchi@sscu.iisc.ernet.in

II. COMPUTATIONAL DETAILS

Micro canonical ensemble molecular dynamics (MD) simulations are carried out in three dimensions on a system of Lennard-Jones particles of mean diameter $\bar{\sigma}$ with polydispersity in both size and mass. The polydispersity in size is introduced by random sampling from the Gaussian distribution of particle diameters σ,

$$P(\sigma) = \frac{1}{\sqrt{2\pi}\delta}\exp\left[-\frac{1}{2}\left(\frac{\sigma-\bar{\sigma}}{\delta}\right)^2\right]. \quad (1)$$

The standard deviation δ of the distribution divided by its mean $\bar{\sigma}$ gives a dimensionless parameter, the polydispersity index, S

$$S = \frac{\delta}{\bar{\sigma}}. \quad (2)$$

The mass m_i of particle i is scaled by its diameter,

$$m_i = \bar{m}\left(\frac{\sigma_i}{\bar{\sigma}}\right)^3. \quad (3)$$

We have chosen $\bar{m}=1.0$. The simulations are carried out at different values of the polydispersity index, S but at fixed volume fraction, $\phi=0.54$. Three different system sizes were chosen, $N=256$, 500, and 864. The results are found to be qualitatively the same for the three different system sizes studied.

The interactions between the particles are given by the shifted-force LJ potential

$$U_{ij} = 4\epsilon_{ij}\left[\left(\frac{\sigma_{ij}}{r_{ij}}\right)^{12} - \left(\frac{\sigma_{ij}}{r_{ij}}\right)^{6}\right], \quad (4)$$

where i and j represent any two particles and

$$\sigma_{ij} = \left(\frac{\sigma_i + \sigma_j}{2}\right). \quad (5)$$

The LJ interaction parameter ϵ_{ij} is assumed to be the same for all particle pairs and set equal to unity. The particles are enclosed in a cubic box and periodic boundary conditions are used. The cutoff radius r_c is chosen to be $2.5\bar{\sigma}$. The time step used for integrating the equations of motion is 0.001. All quantities in this study are given in reduced units [length in units of σ, temperature in units of $\frac{\epsilon}{k_B}$ and time in units of $\tau = (\frac{\bar{m}\bar{\sigma}^2}{\epsilon})^{1/2}$].

The vibrational density of states is obtained from the normal mode analysis by solving the secular equation,

$$|\mathbf{F} - \nu^2\mathbf{I}| = 0. \quad (6)$$

Here F is the mass-weighted potential energy matrix (also known as the Hessian matrix),

$$F_{ij} = \frac{V_{ij}}{\sqrt{m_i m_j}}. \quad (7)$$

Equation (6) can be solved to yield a set of eigenvalues (the square of the vibrational frequencies, ν^2) and corresponding eigenvectors (normal mode displacement vectors), $\mathbf{e}_i$. From the equilibrium liquid configurations generated by the MD simulations, one constructs the potential energy minima or the inherent structure via conjugate gradient minimization. From the potential energy minima, one generates the Hessian matrix, the diagonalization of which would yield the eigenvalues and the eigenvectors. The normal modes thus obtained are called the *quenched normal modes* (QNM).

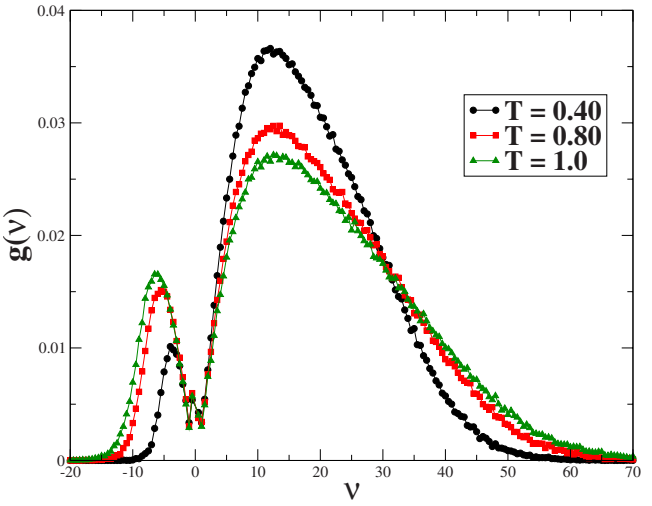

FIG. 1. (Color online) Instantaneous normal mode spectra for different values of T. Data shown for $S=0.10$ system and system size, $N=256$. Unstable modes are shown on the negative frequency axis, i.e., $\nu \equiv \mathrm{sgn}(\lambda)\times\sqrt{|\lambda|}$ [24].

Instantaneous normal modes (INM) can be obtained by diagonalizing the Hessian constructed for the equilibrium liquid configurations. Since the instantaneous liquid configuration is not necessarily a potential energy minimum, one gets both unstable modes (negative eigenvalues or imaginary frequencies) and stable modes (positive eigenvalues).

III. RESULTS AND DISCUSSION

A. Instantaneous normal modes

In Fig. 1, we plot the instantaneous normal mode density of states for different values of temperature T. The imaginary modes are shown in the negative frequency region as per convention. As the temperature decreases, the fraction of the unstable modes decreases whereas that of the stable modes increases. At low temperature ($T=0.40$), the fraction of the unstable modes is considerably less, indicating that most of the particles are located near the potential energy minima most of the time. The polydispersity-dependence of the INM spectra is shown in Fig. 2(a). The $S=0.20$ system has relatively higher number of high-frequency modes for both the stable and unstable branches. The higher fraction of stable high-frequency modes ($\nu>50.0$) for $S=0.20$ is due to the mass polydispersity effect and disappears when the latter is switched off [see Fig. 2(b)]. The polydispersity effects on vibrational modes are discussed in detail in Sec. III B.

B. Quenched normal modes and polydispersity effects on vibration spectra

The configuration-averaged vibrational density of states, $g(\nu)$ for the quenched normal modes is shown in Fig. 3 for

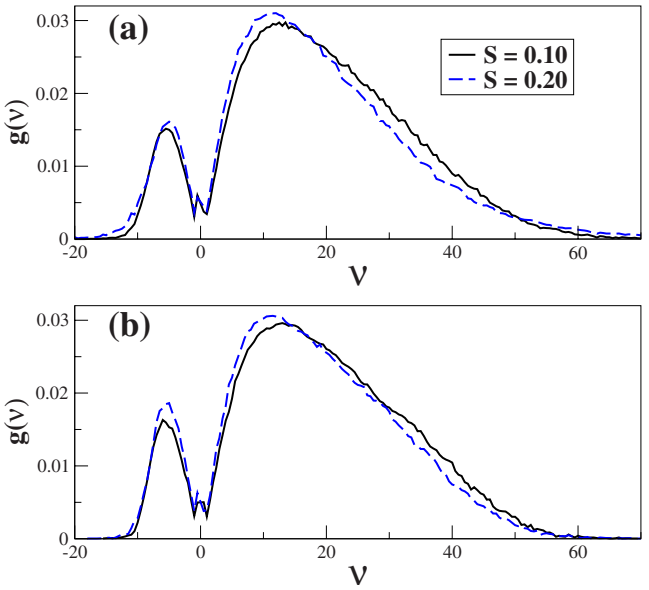

FIG. 2. (Color online) Instantaneous normal mode spectra at $T=0.80$ for $S=0.10$ and $S=0.20$ systems (a) with mass polydispersity (b) without mass polydispersity.

different values of polydispersity index, S. The width of the bin chosen to build the histogram is 0.50. The VDOS is rather featureless as has been observed by Rahman *et al.* [25] for single-component Lennard-Jones system. In Fig. 4, we show the quenched normal mode density of states for $S=0.20$ system for different values of temperature of the parent liquid. The rather narrow sensitivity of the quenched normal mode spectra to temperature is to be contrasted with the INM spectra obtained from equilibrium liquid configurations (see Fig. 1).

Polydispersity has three noticeable effects on the vibrational density of states. First, as polydispersity increases, the number of low-frequency modes increases with a corresponding decrease in the number of high-frequency modes (see Fig. 5). Because of these compensating changes occurring in the high- and low-frequency regions, one observes a crossover in the density of states between $S=0.10$ and $S=0.20$ systems. For the data shown in Fig. 5, this happens at a frequency $\nu \sim 12.0$ for systems with mass polydispersity and $\nu \sim 16.0$ for systems without mass polydispersity. The crossover is reminiscent of an isosbestic point.

Second, when mass polydispersity is present, there is a second crossover point in the density of states between $S=0.10$ and $S=0.20$ systems at a frequency, $\nu \sim 32$ [Fig. 5(a)]. For frequencies higher than this value, there is an excess of high-frequency modes that increases with S. This is best seen

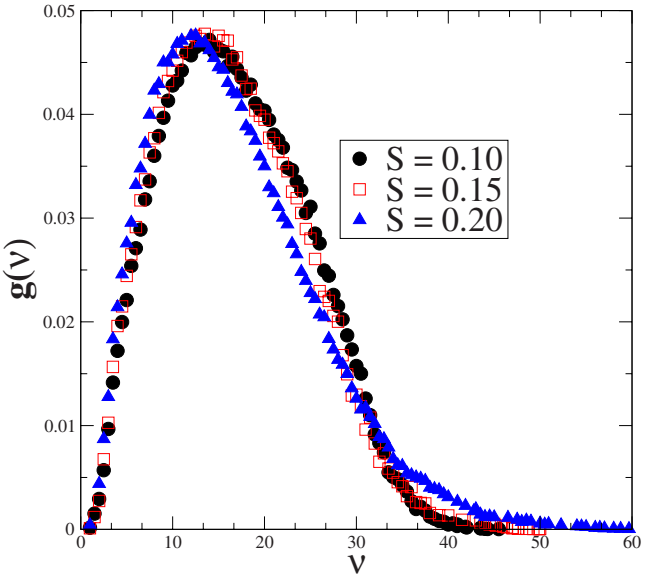

FIG. 3. (Color online) Quenched normal mode spectra at three different values of polydispersity index, S. The data is for $T=0.50$.

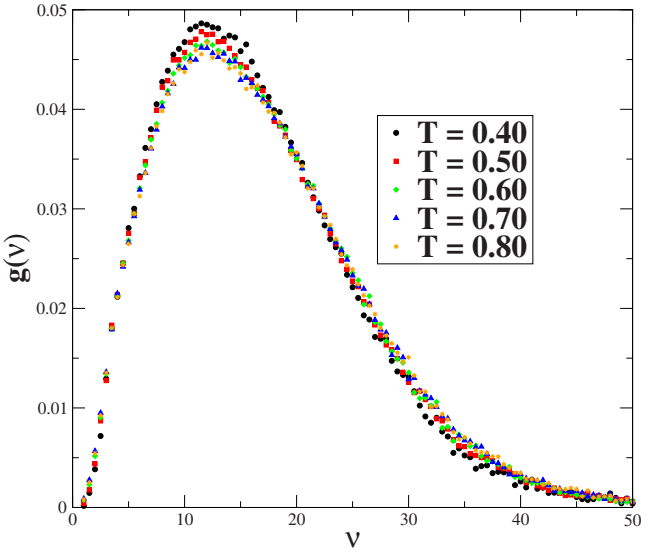

FIG. 4. (Color online) Quenched normal mode spectra at different values of T; data is for $S=0.20$.

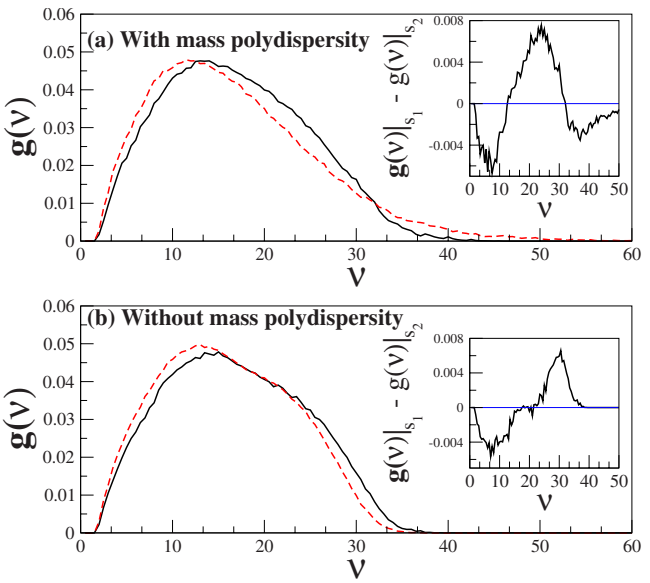

FIG. 5. (Color online) (a) $g(\nu)$ for $S=0.10$ (thick lines) and $S=0.20$ (dashed lines) systems and their difference (inset) (b) Same as (a) but for $S=0.10$ and $S=0.20$ systems without mass polydispersity. Data shown for a system of $N=256$ particles.

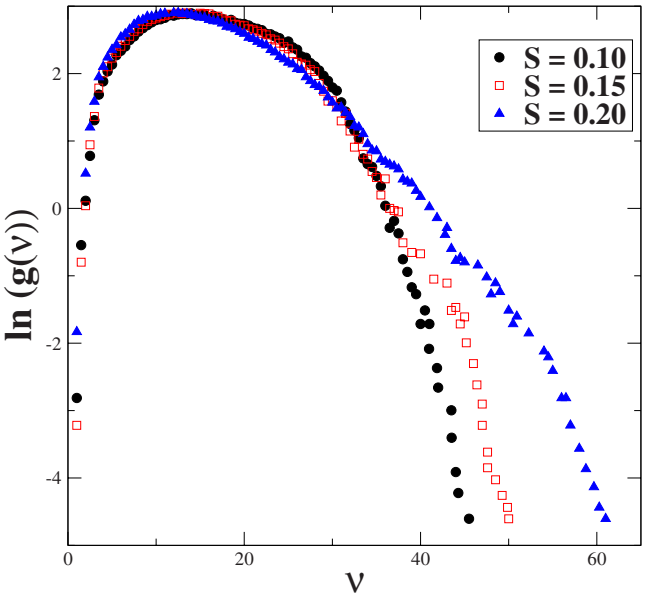

FIG. 6. (Color online) Semilog plot of density of states. The data is for $T=0.50$. As S increases the number of high-frequency modes increases. The high-frequency modes are localized modes (see Fig. 9).

in the semilog plot of $g(\nu)$ in Fig. 6. The plot clearly shows there is a substantial increase in the number of high-frequency modes with S. This feature disappears in the absence of mass polydispersity as shown in Fig. 7. Thus the excess high-frequency modes (whose fraction increases with polydispersity) is due to the mass polydispersity effect rather than size polydispersity effect. In Sec. III C, we show that the high-frequency vibrations are all localized.

Third, the vibrational density of states spectrum becomes narrower with polydispersity. In Fig. 8, we plot the full width at half maximum (FWHM) of $g(\nu)$ for $S=0.10$ and $S=0.20$

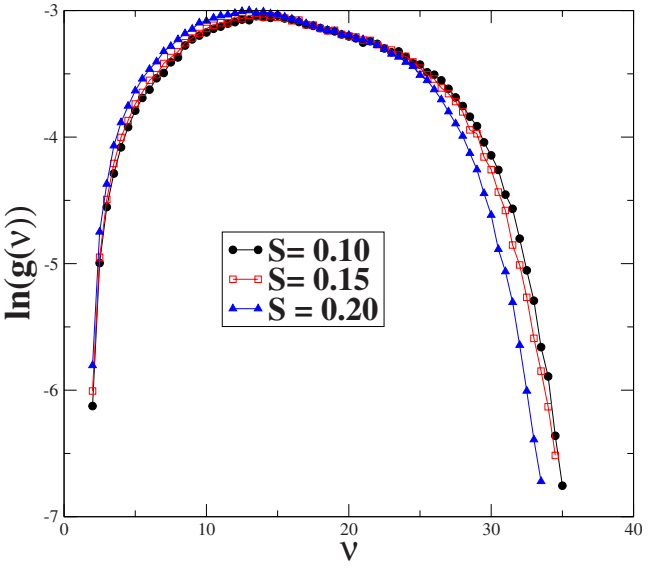

FIG. 7. (Color online) Semilog plot of density of states for different S without mass polydispersity. (i.e., all masses set equal to unity, $m_i=1.0$). The data is for $T=0.50$ and $N=256$.

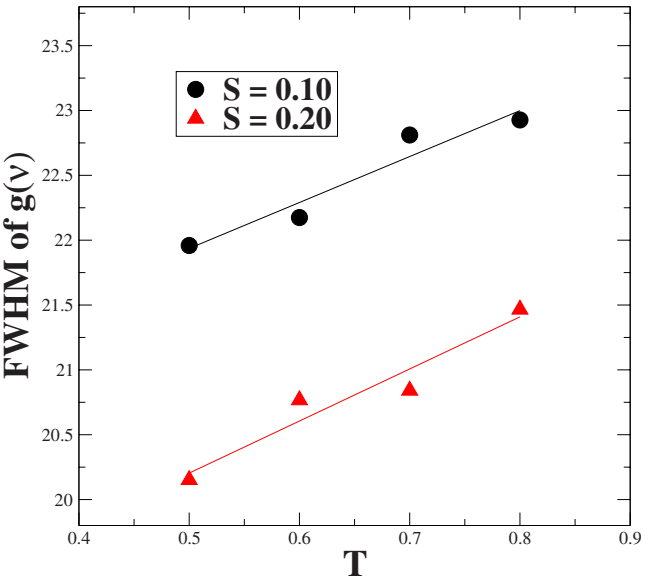

FIG. 8. (Color online) Full width at half maximum, FWHM for $S=0.10$ and $S=0.20$ as a function of T.

as function of T. The FWHM decreases sharply with S but shows only a weak increase with temperature.

C. Polydispersity and localization of normal modes

The localization properties of the normal modes can be quantified via the participation ratio (PR), which is a measure of the number of particles participating in a given vibrational mode. The participation ratio of mode i is defined as

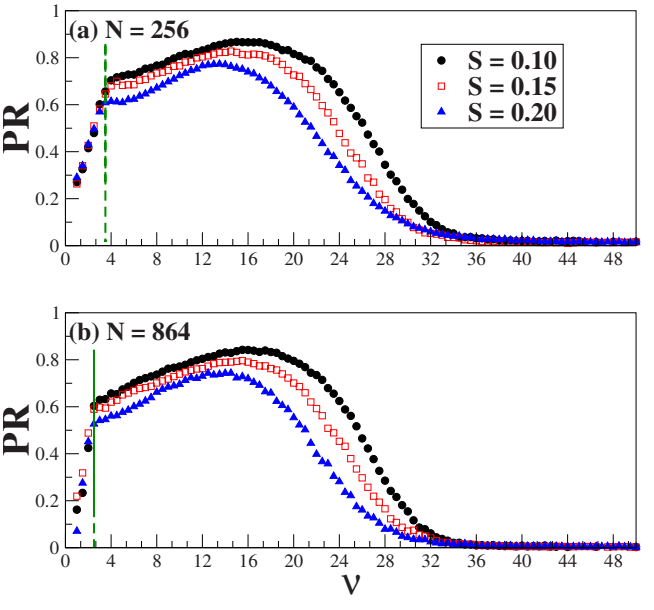

FIG. 9. (Color online) Participation ratio (PR) of the modes for system sizes, (a) $N=256$ and (b) $N=864$. PR gives the number of particles participating in a given mode. The data is shown for different S at $T=0.50$. The plot shows that as S increases, the number of particles participating in a given mode decreases for any given frequency. Dashed line indicates the position of the boson peak.

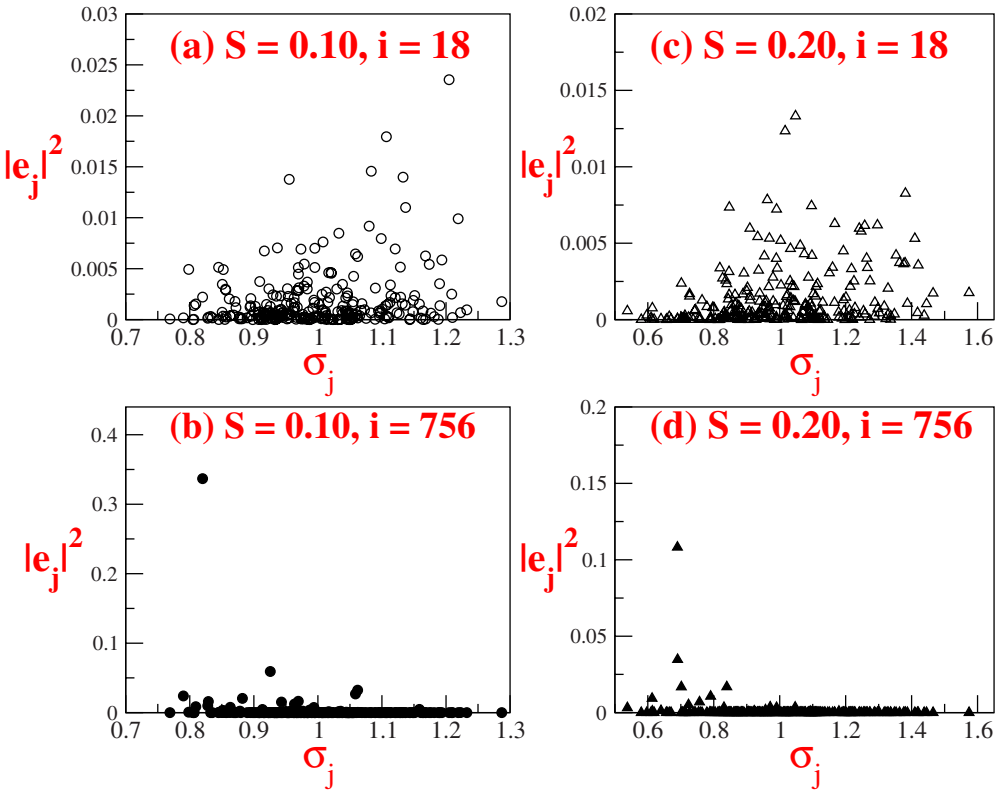

FIG. 10. (Color online) Individual particle displacements in a eigenmode. The index $i=1,\ldots,3N$ and $j=1,\ldots,N$ label the eigenmode and the particle number, respectively. Data shown for $N=256$. (a) An eigenmode near the maximum frequency for $S=0.10$ system. (b) A high-frequency eigenmode for $S=0.10$ system. (c) An eigenmode near the maximum frequency for $S=0.20$ system. (d) A high-frequency eigenmode for $S=0.20$ system.

$$\mathrm{PR}_i = \left[N \sum_{\alpha=1}^{3N} (e_i^\alpha \cdot e_i^\alpha)^2 \right]^{-1} \tag{8}$$

Thus, PR is of the order of $\frac{1}{N}$ for localized modes and is on the order of 1 for extended modes. In Fig. 9, the participation ratio of the modes is plotted. The averaging is done over modes corresponding to eigenvalues in a histogram bin of width 0.50. For $\nu > 30.0$, the participation ratio is very low. Thus, the high-frequency tail of the normal mode spectrum is due to localized vibrations. This is depicted in Fig. 10, where we plot the individual particle displacements in an eigenmode from the high-frequency side as well as one near the frequency at which $g(\nu)$ shows a maximum. The figure clearly shows that the high-frequency vibrations are localized on lighter particles. In a crystalline solid, localized vibrations occur due to the presence of very light impurity atoms or interstitial atoms. It has been shown that when the mass of the impurity atom in a crystal is smaller than that of the other particles, the vibrations do not propagate through the system but gets localized around the impurity particle [26].

In the frequency range $3.0 \leq \nu \leq 35$, one finds delocalized modes as implied by the high values of PR. The participation ratio of the modes decreases with polydispersity for modes of all frequencies (see Fig. 9). Thus, the vibrations become more localized with S. This means that as size disparity among the particles increases, the system cannot sustain propagating modes. It is interesting to note here that the large size disparity among the particles also leads to the suppression of growth of dynamic heterogeneity with polydispersity in supercooled liquids. Dynamic heterogeneity in supercooled liquids in its simplest sense means clusters of fast-moving particles that move together for a certain amount of time before they get decorrelated. When size disparity is large, the particle motion gets decorrelated much faster and hence the formation of *dynamic* clusters is suppressed at higher polydispersity.

D. Boson peak

We plot the reduced density of states, $g(\nu)/\nu^2$ in Fig. 11 for three values of S, namely, $S=0.10$, 0.15, and 0.20. All the three systems exhibit the boson peak feature viz. excess density of states as compared to the prediction of the Debye model, $g(\nu) \sim \nu^2$. The boson peak feature is seen even when we switch off the mass polydispersity [see Fig. 11(b)] implying that the size polydispersity effect alone can give rise to the observed features. As seen from the figure, the intensity of the boson peak, I_{BP} increases with S for all the three system sizes studied. However, *there is no noticeable change in the frequency of the Boson peak*, ν_{BP} with S. The position of the boson peak and its height show a strong system size dependence. The peak height increases with system size and the peak shifts to lower frequencies, the values of ν_{BP} being 3.5, 3.0, and 2.5 for $N=256$, 500, and 864, respectively.

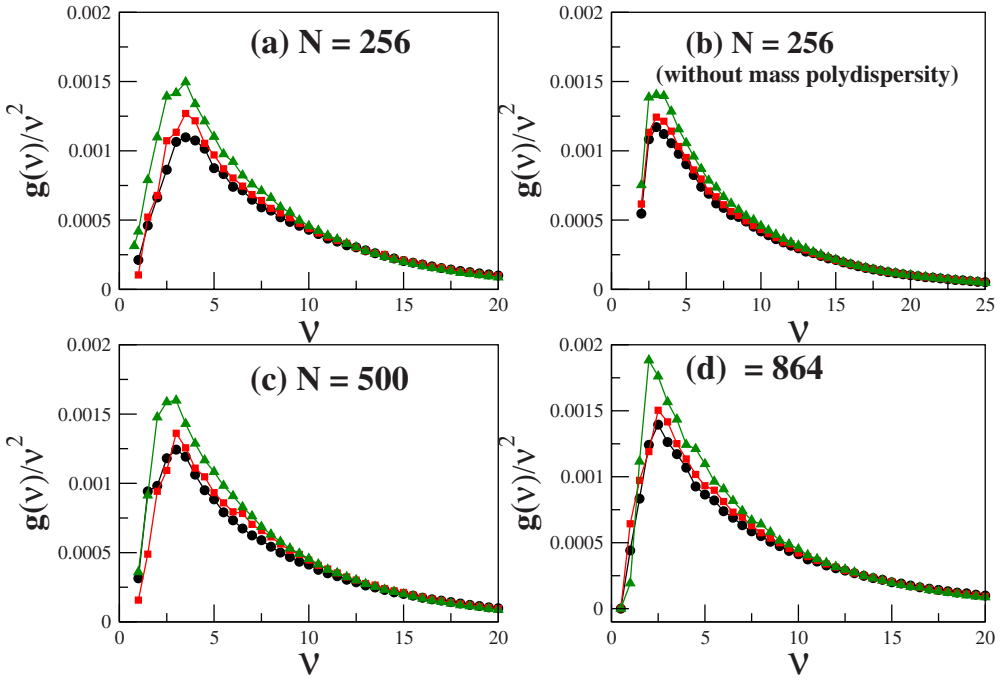

FIG. 11. (Color online) Excess density of states (Boson Peak), $\frac{g(\nu)}{\nu^2}$ versus ν. Data shown for different S with the temperature of the parent liquid at $T=0.50$ and for system sizes, (a) $N=256$ (b) $N=256$ but without mass polydispersity (c) $N=500$ and (d) $N=864$. If we choose Argon units, the frequency of boson peak is in the range $\nu_{BP} \sim 1.1-3.5\times 10^{12}$ s^{-1}.

Simulations of much larger system sizes are required to fully understand the finite size effects. However the polydispersity-dependence of the boson peak spectrum, which is one of the main goals of the current study, is qualitatively the same for the three different system sizes studied here.

The boson peak feature is seen even for the quenched normal modes obtained from equilibrium configurations at very high temperature (i.e., $T \gg T_{MCT}$), as shown in Fig. 12. As T increases, the boson peak height increases but the peak shifts to lower frequencies. Such a trend has been observed in experiments as well [27,28]. However, the temperature-dependence is weak here. The boson peak feature at high temperatures shown in Fig. 12 is to be contrasted with the observation made in an earlier paper [12] where the authors studied the appearance of the boson peak in soft sphere binary mixture. In their study, the authors found that as T increases above T_{MCT}, the boson peak feature disappears. The authors interpret the boson peak as a manifestation of an underlying crossover of the parent liquid's configuration from a saddle dominated dynamics to a minima-dominated behavior. However, the observation of boson peak at high temperatures makes such an interpretation questionable.

The fragility of the current model polydisperse supercooled liquid decreases with polydispersity. This suggests an inverse correlation between the fragility of the liquid and the intensity of the boson peak. Such a correlation has actually been observed previously for many liquids in experiments [29] as well as in the simulation studies of model glass formers [14]. If a correlation between the fragility and the intensity of the boson peak exists, then it would mean that there is also a link between the fast intrabasin vibrational dynamics and the slow interbasin diffusive dynamics (see [30]). However, it appears hard to reconcile such a *link* with the Adam-Gibbs paradigm as the latter predicts a relationship between the relaxation time, τ and the configurational entropy, S_c [$\tau \sim \exp(\frac{A}{TS_c})$]. Clearly, on the time scale typical of vibrational dynamics (few picoseconds), the system would not have sampled sufficient configurations as would be necessary to define S_c. Hence, it is difficult to understand the correlation between the intensity of the boson peak and fragility from this perspective.

It is interesting to note in this connection that Angell *et al.* [31] have already suggested that the Boson peak can serve as

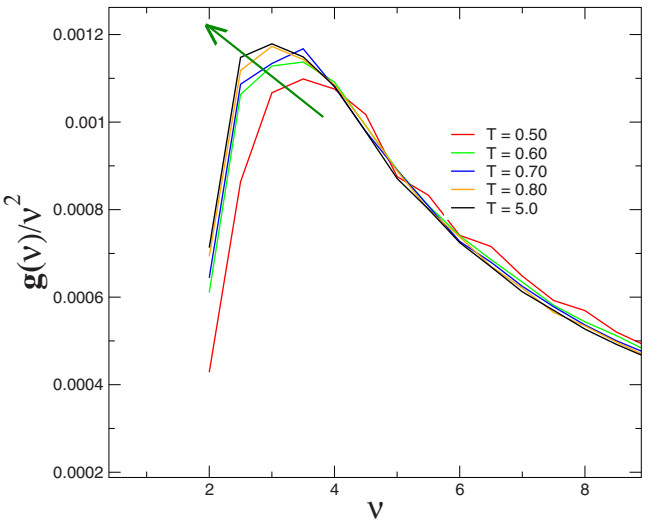

FIG. 12. (Color online) Temperature dependence of the Boson Peak. The data is shown for $S=0.10$ for different temperatures of the parent liquid.

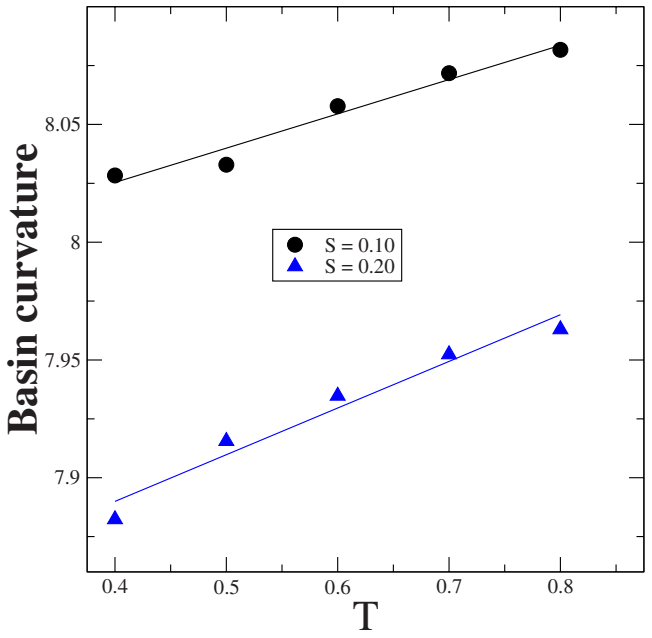

FIG. 13. (Color online) Basin curvature as a function of temperature for $S=0.10$ and $S=0.20$ systems.

a signature of configurational excitations of the ideal glass structure, i.e., the topologically diverse defects of the glassy solid state. This means that the boson peak is related to the topographical features of the potential energy landscape and is thus involved in determining the fragility of the liquid. In the inherent structure formalism developed by Stillinger and Weber [32,33], the configuration space of the liquid is divided into basins of local potential energy minima (or inherent structures). Within the harmonic approximation, valid at sufficiently low temperatures, each basin is treated as a harmonic well. In Fig. 13, we plot the quantity $N^{-1}\Sigma_{k=1}^{3N-3}\log(h\nu_k)$ as a function of T for $S=0.10$ and $S=0.20$ systems. This quantity is an indicator of the average curvature of the basins [34]. Thus at higher polydispersity we have *flatter* basins, which is consistent with the decrease of fragility with S, as fragile liquids have rugged heterogeneous landscape whereas strong liquids have smoother landscapes, in accord with their constant activation energy predicted by their Arrhenius behavior. The strong liquids in Angell's fragile/strong classification are usually network glass formers like SiO_2, GeO_2 etc., and they appear to lie almost on the opposite spectrum of our polydisperse liquid system. For a polydisperse LJ liquid, the decrease in fragility with polydispersity is via dynamic facilitation by smaller particles. An obvious manifestation of the dynamic facilitation is the size-dependent glass transition temperature; as temperature is lowered the larger particles freeze in first, followed by the smaller ones. Therefore dynamic facilitation by polydispersity implies that at higher polydispersity not only the system has smaller barriers to diffusion but it also has more relaxation channels available to it.

Here it is interesting to note that Shirmacher *et al.* [9] have shown that if a system of coupled harmonic oscillators (with spatially fluctuating nearest-neighbor force constants on a simple cubic lattice) is near the borderline of stability a low-frequency peak appears in $g(\nu)/\nu^2$ as a precursor of the instability. In their model system, when the amount of the negative force constants becomes too large, the system becomes unstable and the boson peak feature shows up. Furthermore, as the fraction of negative force constants increases the peak intensity increases and the peak shifts toward lower frequencies. Instantaneous normal mode analysis shows (see again Fig. 2) that the fraction of unstable modes increases with polydispersity which implies more pathways for diffusion [16] at higher polydispersity.

E. Are the modes comprising the boson peak localized or extended?

One of the key issues in the interpretation of the boson peak is whether the modes comprising it are localized or extended. In this study, we mainly use the participation ratio and level spacing statistics to address this issue.

1. Participation ratio

Figure 9 shows that the modes at the frequency range where boson peak appears are largely delocalized with high values of participation ratio (PR$>$0.5). For frequencies less than ν_{BP}, the participation ratio drops suddenly. This sudden drop of PR at low frequencies has been attributed to finite size effects [18]. These low-frequency modes have been shown to be extended, notwithstanding their low PR values. However, note that the frequency of the boson peak coincides with the frequency below which PR suddenly drops. Furthermore, at the boson peak frequency, the PR decreases with S indicative of a correlation between localization of modes and boson peak intensity. These features are common to all the three system sizes ($N=256$, 500 and 864) studied.

2. Level spacing statistics

An alternate way to check whether the boson peak is indeed associated with localized modes (or not) is by means of level distance statistics [9,35]. The level spacing distribution, $P(s)$ for the random-matrix models is defined as the probability of finding the next-nearest-neighbor eigenvalue of the spectrum to be at a distance s, i.e., $s=\frac{\lambda_{i+1}-\lambda_i}{D}$, where D is the mean level spacing. In the case of delocalized states, according to the Gaussian orthogonal random-matrix ensemble, we get

$$P(s) = As^{\beta}\exp(-Bs^2). \tag{9}$$

For localized states, one gets a Poisson distribution,

$$P(s) = \exp(-s). \tag{10}$$

This is due to the fact that the delocalized states show level repulsion, whereas localized ones do not.

In order to characterize the level spacing distribution, we use the Brody function $P_\beta(s)$ to fit the computed distribution [36,37]

$$P_\beta(s) = c_1 s^{\beta}\exp(-c_2 s^{\beta+1}), \tag{11}$$

with

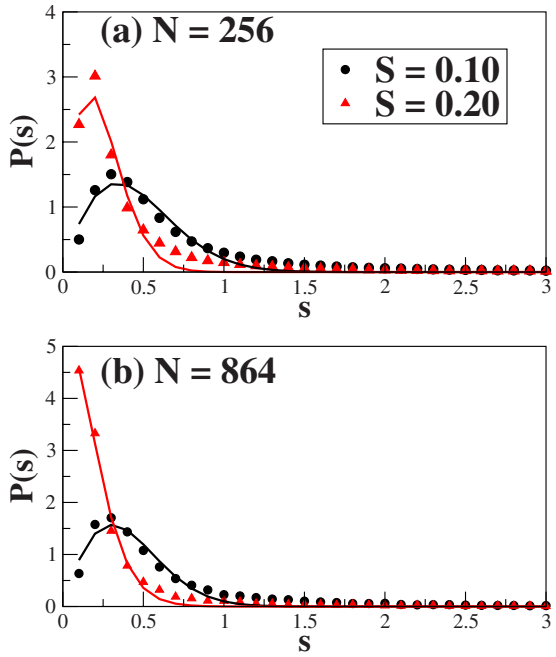

FIG. 14. (Color online) The level spacing distribution, $P(s)$ for the full eigenvalue spectrum. Data is shown for $S=0.10$ (circles) and $S=0.20$ (triangles) systems at $T=0.60$. Upper panel is for system size, $N=256$ and lower panel for $N=864$. The symbols are the data points and the thick lines are fit to the data according to Eq. (11). Fit parameters are given in Table I.

$$c_2 = \left[\Gamma\left(\frac{\beta+2}{\beta+1}\right)\right]^{\beta+1} \tag{12}$$

and

$$c_1 = (\beta+1)c_2. \tag{13}$$

In this function, β represents the degree of the distribution $P(s)$: the value of $-0.1<\beta<0.1$ corresponds to a Poisson distribution, while the value of $0.5<\beta<1.2$ to a Wigner distribution of the Gaussian orthogonal ensemble.

In Fig. 14, we have plotted the level spacing distribution $P(s)$ for the full eigenvalue spectrum along with the fit for the Eq. (11). The fit parameters are given in Table I. It appears that the level spacing distribution for both $S=0.10$ and $S=0.20$ for the system size, $N=256$ agrees with Wigner's surmise with β value being 0.834 and 0.729, respectively. However, at the larger system size studied ($N=864$), β for

TABLE I. The values of the fit parameters obtained by fitting Eq. (11) to the full eigenvalue spectrum.

N	S	c_1	β	c_2
256	0.10	5.287	0.834	3.277
256	0.20	15.44	0.729	9.312
864	0.10	7.031	0.872	4.276
864	0.20	15.178	0.345	8.917

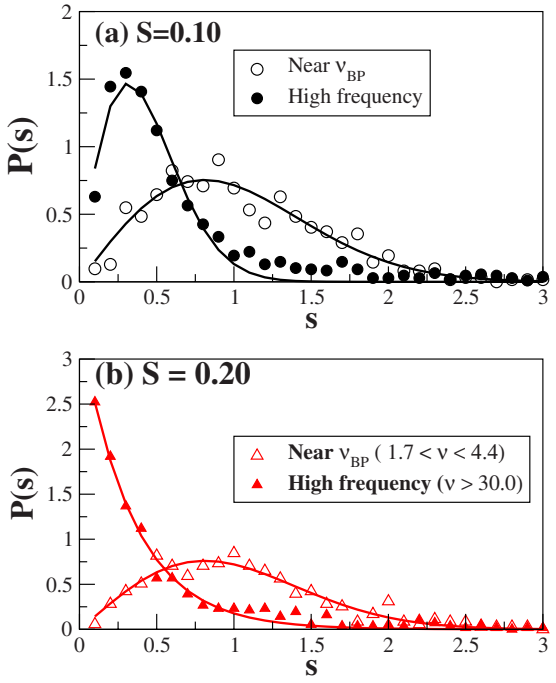

FIG. 15. (Color online) The level spacing distribution, $P(s)$ for the eigenvalues in the range $1.7\leq\nu\leq4.4$ (near the boson peak) shown in open symbols and for eigenvalues in the high-frequency range ($\nu>35.0$) shown by filled symbols. Data is shown for (a) $S=0.10$ and (b) $S=0.20$ at $T=0.60$ and $N=864$. The symbols are the data points and the thick lines are fit to the data according to Eq. (11). Fit parameters are given in Table II.

$S=0.20$ system is 0.345, indicating that the $S=0.20$ system shows some mixture of both Poisson and Wigner distribution.

To see whether the modes comprising the boson peak are localized or not, in Fig. 15, we plot the level spacing distribution for frequencies near the boson peak ($1.7\leq\nu\leq4.4$). Also shown in the figure is the level spacing distribution for the high frequencies ($\nu>30.0$) where the modes are truly localized (See 9). The fit parameters are given in Table II. From the plot, it is clear that statistics at high frequencies follow Poisson distribution as expected for localized states. In the vicinity of the boson peak, however, we find a distribution according to the Gaussian Orthogonal Ensemble, which means that the corresponding states are delocalized. It is interesting to note that even though the full eigenvalue spectrum for $S=0.20$ system shows predominantly Poisson behavior that is characteristic of localized modes, the modes

TABLE II. The values of the fit parameters obtained by fitting Eq. (11) to the eigenvalues near the boson peak and for those in the high-frequency range (where modes are truly localized).

ν	S	c_1	β	c_2
Near ν_{BP}	0.10	1.537	1.001	0.765
Near ν_{BP}	0.20	1.572	1.037	0.779
$\nu>30.0$	0.10	6.124	0.839	3.842
$\nu>30.0$	0.20	2.847	−0.095	2.579

near boson peak for this system follow the Wigner surmise of delocalized modes.

Although both the participation ratio and the level spacing statistics of the finite size systems studied here seem to indicate that these modes are delocalized (it is likely that these modes are delocalized over a few hundred particles), it is unlikely that these modes are delocalized over an entire macroscopic system. Note that participation ratio decreases with system size, implying increasing localization, which is also reflected in the level spacing distribution. The latter becomes more Poisson-like with increase in system size. The sudden drop of participation ratio at the boson peak frequency indicates that the low-frequency vibrations are quasilocalized vibrations (QLVs). The QLVs are the local low-frequency vibrations involving several atoms that are bilinearly coupled to the sound waves [38]. Parshin *et al.* [39] has proposed a mechanism for boson peak formation based on the phenomenon of vibrational instability arising from the interaction of the QLVs with the high-frequency vibrations. According to this theory the vibrational instability of weakly interacting harmonic oscillators are responsible for both the formation of two-level systems and the boson peak in reduced density of states.

IV. CONCLUDING REMARKS

Let us first summarize the main results of this paper. We have computed the vibrational density of states in a polydisperse Lennard-Jones system. Polydispersity is shown to have a significant effect on the vibrational density of states. Increase in the polydispersity leads to an increase in the localized high-frequency modes. There is a softening of vibrational modes with polydispersity manifested in the population shift in modes with frequencies above the maximum in $g(\nu)$ to that below the maximum. The reduced density of states, $g(\nu)/\nu^2$ exhibits the boson peak feature. The latter is seen to exist even for high-temperature liquid configurations and shows a rather narrow sensitivity to temperature. The results clearly show a correlation between the height of the BP and the strength of the liquid.

The observed weak temperature-dependence of the boson peak seems to suggest the absence of any temperature mediated phase transition in the stationary points of the energy landscape from a saddle dominated to a minima-dominated regime. We find that while the modes comprising the BP are largely delocalized, there is a sharp drop in the PR of the modes that exist just below the BP. We also find a correlation between localization of modes and boson peak intensity. These results suggest that the low-frequency modes could be quasilocalized vibrations. All these evidences do suggest a close relation between boson peak and unstable modes of the system, the latter being responsible for the facilitation of relaxation at larger polydispersity as well as the observed softening of vibrational modes with polydispersity. Possible candidates of the modes populating boson peak are therefore modes that are connected with two-level systems [39] but in a strongly correlated system like a glass or a supercooled liquid, a transition in a two-level system may involve participation of a large number of particles, and this could explain the relatively large value of the participation ratio. These modes populate the saddles of the energy landscape [12], as also evident from INM analysis.

[1] F. Sette *et al.*, Science **280**, 1550 (1998).
[2] *Amorphous Solids-Low Temperature Properties*, Topics in Current Physics Vol. 24, edited by W. A. Philips (Springer-Verlag, Berlin, 1981).
[3] T. Nakayama, Physica B **263-264**, 243 (1999).
[4] W. Schirmacher, Europhys. Lett. **73**, 892 (2006).
[5] A. I. Chumakov, I. Sergueev, U. van Burck, W. Schirmacher, T. Asthalter, R. Ruffer, O. Leupold, and W. Petry, Phys. Rev. Lett. **92**, 245508 (2004).
[6] C. Oligschleger and H. R. Schober, Phys. Rev. B **59**, 811 (1999).
[7] Yu. G. Vainer, A. V. Naumov, M. Bauer, and L. Kador, Phys. Rev. Lett. **97**, 185501 (2006).
[8] V. L. Gurevich, D. A. Parshin, and H. R. Schober, JETP Lett. **76**, 553 (2002).
[9] W. Schirmacher, G. Diezemann, and C. Ganter, Phys. Rev. Lett. **81**, 136 (1998).
[10] H. Cang, J. Li, H. C. Anderson, and M. D. Fayer, J. Chem. Phys. **123**, 064508 (2005).
[11] F. Leonforte, R. Boissiere, A. Tanguy, J. P. Wittmer, and J.-L. Barrat, Phys. Rev. B **72**, 224206 (2005).
[12] T. S. Grigera, V. Martin-Mayor, G. Parisi, and P. Verrocchio, Nature (London) **422**, 289 (2003).
[13] V. Lubchenko and P. G. Wolynes, Proc. Natl. Acad. Sci. U.S.A. **100**, 1515 (2003).
[14] H. Shintani and H. Tanaka, Nature Mater. **7**, 870 (2008).
[15] S. R. Nagel, G. S. Grest, and A. Rahman, Phys. Rev. Lett. **53**, 368 (1984).
[16] R. A. LaViolette and F. H. Stillinger, J. Chem. Phys. **83**, 4079 (1985).
[17] B. B. Laird and H. R. Schober, Phys. Rev. Lett. **66**, 636 (1991).
[18] V. Mazzacurati, G. Ruocco, and M. Sampoli, Europhys. Lett. **34**, 681 (1996).
[19] E. R. Weeks *et al.*, Science **287**, 627 (2000).
[20] S. C. Glotzer, V. N. Novikov, and T. B. Schroder, J. Chem. Phys. **112**, 509 (2000).
[21] R. K. Murarka and B. Bagchi, Phys. Rev. E **67**, 051504 (2003).
[22] S. E. Abraham, S. M. Bhattacharrya, and B. Bagchi, Phys. Rev. Lett. **100**, 167801 (2008).
[23] S. E. Abraham and B. Bagchi, Phys. Rev. E **78**, 051501 (2008).
[24] M. Cho, G. R. Fleming, S. Saito, I. Ohmine, and R. Stratt, J. Chem. Phys. **100**, 6672 (1994).
[25] A. Rahman, M. J. Mandell, and J. P. McTague, J. Chem. Phys. **64**, 1564 (1976).
[26] E. I. Takizawa and L. Kobayashi, Chin. J. Phys. **5**, 11 (1967).

[27] N. J. Tao, G. Li, X. Chen, W. M. Du, and H. Z. Cummins, Phys. Rev. A **44**, 6665 (1991).
[28] D. Engberg, A. Wischnewski, U. Buchenau, L. Borjesson, A. J. Dianoux, A. P. Sokolov, and L. M. Torell, Phys. Rev. B **59**, 4053 (1999).
[29] V. N. Novikov, Y. Ding, and A. P. Sokolov, Phys. Rev. E **71**, 061501 (2005).
[30] T. Scopigno *et al.*, Science **302**, 849 (2003).
[31] C. A. Angell, Y. Yue, L. Wang, J. R. D. Copley, S. Borick, and S. Mossa, J. Phys.: Condens. Matter **15**, S1051 (2003).
[32] F. H. Stillinger and T. A. Weber, Science **225**, 983 (1984).
[33] F. H. Stillinger, Science **267**, 1935 (1995).
[34] S. Mossa, E. La Nave, H. E. Stanley, C. Donati, F. Sciortino, and P. Tartaglia, Phys. Rev. E **65**, 041205 (2002).
[35] F. M. Izrailev, Phys. Rep. **196**, 299 (1990).
[36] K. Fukui, B. G. Sumpter, D. W. Noid, C. Yang, and R. E. Tuzun, Comput. Theor. Polym. Sci. **11**, 191 (2001).
[37] H. Meyer, J.-C. Angles d'Auriac, and J.-M. Maillard, Phys. Rev. E **55**, 5380 (1997).
[38] H. R. Schober and G. Ruocco, Philos. Mag. **84**, 1361 (2004).
[39] D. A. Parshin, H. R. Schober, and V. L. Gurevich, Phys. Rev. B **76**, 064206 (2007).